NOAA Technical Report ERL 312-WPL 35

U.S. DEPARTMENT OF COMMERCE
NATIONAL OCEANIC AND ATMOSPHERIC ADMINISTRATION
Environmental Research Laboratories

Theoretical Analysis and Experimental Evaluation of a Prototype Passive Sensor to Measure Crosswinds

S. F. CLIFFORD
G. R. OCHS
TING-I WANG

BOULDER, COLO.
SEPTEMBER 1974

ENVIRONMENTAL RESEARCH LABORATORIES

The mission of the Environmental Research Laboratories is to study the oceans, inland waters, the lower and upper atmosphere, the space environment, and the earth, in search of the understanding needed to provide more useful services in improving man's prospects for survival as influenced by the physical environment. Laboratories contributing to these studies are:

Atlantic Oceanographic and Meteorological Laboratories (AOML): Geology and geophysics of ocean basins and borders, oceanic processes, sea-air interactions and remote sensing of ocean processes and characteristics (Miami, Florida).

Pacific Marine Environmental Laboratory (PMEL): Environmental processes with emphasis on monitoring and predicting the effects of man's activities on estuarine, coastal, and near-shore marine processes (Seattle, Washington).

Great Lakes Environmental Research Laboratory (GLERL): Physical, chemical, and biological limnology, lake-air interactions, lake hydrology, lake level forecasting, and lake ice studies (Ann Arbor, Michigan).

Atmospheric Physics and Chemistry Laboratory (APCL): Processes of cloud and precipitation physics; chemical composition and nucleating substances in the lower atmosphere; and laboratory and field experiments toward developing feasible methods of weather modification.

Air Resources Laboratories (ARL): Diffusion, transport, and dissipation of atmospheric contaminants; development of methods for prediction and control of atmospheric pollution; geophysical monitoring for climatic change (Silver Spring, Maryland).

Geophysical Fluid Dynamics Laboratory (GFDL): Dynamics and physics of geophysical fluid systems; development of a theoretical basis, through mathematical modeling and computer simulation, for the behavior and properties of the atmosphere and the oceans (Princeton, New Jersey).

National Severe Storms Laboratory (NSSL): Torandoes, squall lines, thunderstorms, and other severe local convective phenomena directed toward improved methods of prediction and detection (Norman, Oklahoma).

Space Environment Laboratory (SEL): Solar-terrestrial physics, service and technique development in the areas of environmental monitoring and forecasting.

Aeronomy Laboratory (AL): Theoretical, laboratory, rocket, and satellite studies of the physical and chemical processes controlling the ionosphere and exosphere of the earth and other planets, and of the dynamics of their interactions with high-altitude meteorology.

Wave Propagation Laboratory (WPL): Development of new methods for remote sensing of the geophysical environment with special emphasis on optical, microwave and acoustic sensing systems.

Marine EcoSystem Analysis Program Office (MPO): Plans and directs interdisciplinary analyses of the physical, chemical, geological, and biological characteristics of selected coastal regions to assess the potential effects of ocean dumping, municipal and industrial waste discharges, oil pollution, or other activity which may have environmental impact.

Weather Modification Program Office (WMPO): Plans and directs ERL weather modification research activities in precipitation enhancement and severe storms mitigation and operates ERL's research aircraft.

NATIONAL OCEANIC AND ATMOSPHERIC ADMINISTRATION
BOULDER, COLORADO 80302

U.S. DEPARTMENT OF COMMERCE
Frederick B. Dent, Secretary

NATIONAL OCEANIC AND ATMOSPHERIC ADMINISTRATION
Robert M. White, Administrator
ENVIRONMENTAL RESEARCH LABORATORIES
Wilmot N. Hess, Director

NOAA TECHNICAL REPORT ERL 312-WPL 35

Theoretical Analysis and Experimental Evaluation of a Prototype Passive Sensor to Measure Crosswinds

S. F. CLIFFORD
G. R. OCHS
TING-I WANG

This report was supported in part by the
U. S. Army Electronics Command,
Atmospheric Sciences Laboratory,
White Sands, N. M. 88002, under A43BXL 74-8013.
Mr. T. H. Pries was the ASL Scientific Monitor.

BOULDER, COLO.
September 1974

For sale by the Superintendent of Documents, U. S. Government Printing Office, Washington, D. C. 20402

Printed for Atmospheric Sciences Laboratory,
U.S. Army Electronics Command, White Sands Missile Range,
New Mexico 88002, as Research and Development Technical Report
ECOM-74-3. Approved for public release; distribution unlimited.

TABLE OF CONTENTS

THEORETICAL ANALYSIS AND EXPERIMENTAL EVALUATION OF A PROTOTYPE PASSIVE SENSOR TO MEASURE CROSSWINDS

S. F. Clifford, G. R. Ochs, and Ting-i Wang

We describe and analyze the performance of our prototype passive wind sensor. The instrument interprets the turbulence-induced optical scintillations of a random scene to infer a path-weighted transverse wind speed between scene and observer. We derive the fundamental theoretical relations on which the system is based and discuss the overall capabilities and limitations of the technique. We conclude that the system has useful application but requires a more extensive demonstration of its ability to perform with a wider variety of scene spectra and under more diverse meteorological conditions before the technique becomes operational.

1. INTRODUCTION

The goal for this work is to provide a theoretical and experimental evaluation of a technique for the measurement of the wind component normal to an atmospheric line-of-sight path by analysis of scintillations of light reflected from a target surface at one end of the path and observed from the other end. This report also includes the evaluation of saturation effects on optical wind measurements. A working prototype instrument based upon the above studies was furnished as part of the contract.

The optical technique is basically that proposed in Ochs et al.(1973). It is related to the optical measurement of average wind using a laser acting as a single point source of light but the use of an arbitrary distribution of light in a scene, rather than a point light source, requires a fairly drastic modification of that technique.

In general, for the passive system under consideration, one needs the following inputs:

W, the weighting function desired,

L, the distance to the scene,

$C_n^2(z)$, the distribution of refractive-index turbulence along the path, and

Q^2, the spatial spectrum of the scene.

In principle, the average crosswind, weighted according to W, can be determined by inspection of the scintillation with a suitable receiver. We assume that L is known and W is defined. The weighting function W cannot be completely arbitrary, but a useful variety of weighting functions can be specified. We also assume that C_n^2 is statistically uniform over the path. On a horizontal path, this assumption means that the optical wind measurement does not represent the instantaneous mean wind; rather it is an estimate that becomes more and more accurate as the averaging period becomes longer. A reasonable estimate should be obtained in the time it takes the air to move a distance equal to the length of the optical path. For slant optical paths, C_n^2 is statistically non-uniform and the weighting function will be altered.

The above discussion of W and C_n^2 also applies to the standard optical wind measurement (active system). The additional variable in a passive system is the arbitrary spatial spectrum of the scene. In the active system, using a point laser source, the spatial spectrum is known (it is flat). A typical scene has a different character, as shown in figure 1. Different scenes have surprisingly uniform spectra, although the dropoff with higher spatial frequencies is very different from the flat point-source spectrum.

One of the key problems in devising a passive optical wind measuring system is to develop a practical method for measuring the important characteristics of the spatial spectrum of the scene, and to use this

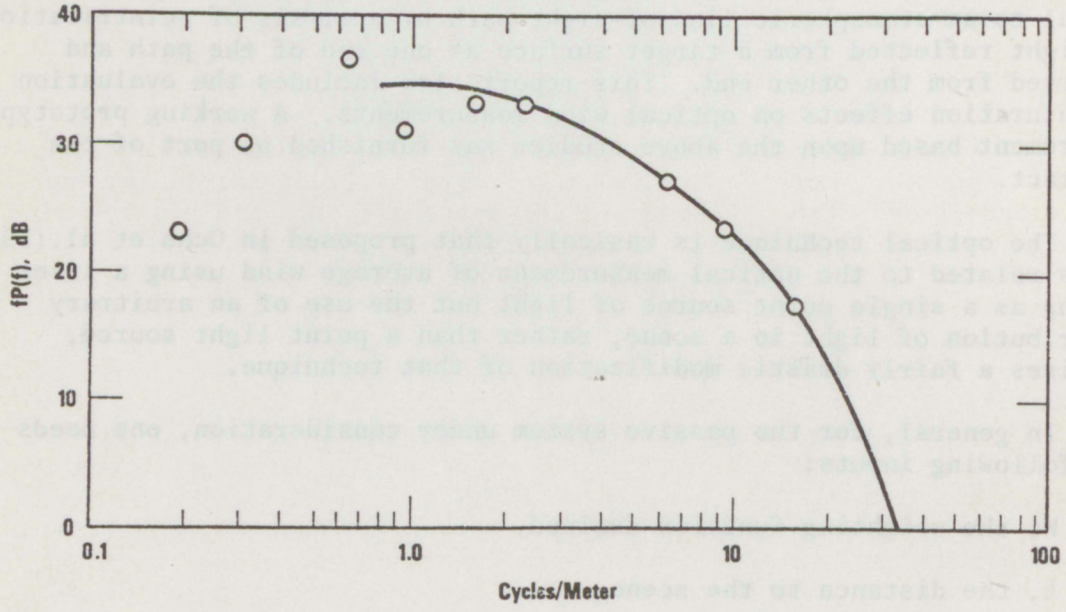

Fig. 1. One-dimensional spatial spectrum of 35 mm color slide showing two vehicles against a background of trees. The abscissa is scaled to actual dimensions at the vehicles.

information to determine the weighting function W and the slope-wind calibration factor CF,[1] which is defined as the ratio of the measured slope at zero time lag to the true wind speed. In general, it is a function of path length, wavelength, and scene spectrum.

We measure the slope of the received spatial spectrum to infer the spatial spectrum of the scene. A lens system is used to avoid the difficulties generated by a secondary obstruction of the aperture. With no adjustments whatsoever, the final instrument gives a reasonably accurate estimate of crosswinds over a range of scene distances and scene spectra. There is enough flexibility in the system, however, so that optimum adjustments may be made for operation at one location.

We will discuss here the two principal techniques investigated. We have called them "broadband" and "narrowband" in accordance with the spatial spectral response of the receiver. Both techniques will work but the narrowband technique has been selected for implementation.

2. THEORY OF PASSIVE WIND SENSING

The general theory of passive wind sensing is derived from the analysis of the propagation geometry of figure 2. A point source of light, located at $(\rho,0)$, illuminates a differential phase screen of wavenumber $\underset{\sim}{K}$ at $\underset{\sim}{r}'=(\rho',z)$ and the scattered field is observed by a detector at $\underset{\sim}{(\rho_1,L)}$. The total field, incident plus scattered, at $z=L$ is, from Lee and Harp (1969)

$$dE = 1 - ik\,a\,dz \exp\left[\frac{iK^2 z(L-z)}{2kL}\right] \cos[\underset{\sim}{K}\cdot\underset{\sim}{\rho}_1(z/L)+\underset{\sim}{K}\cdot\underset{\sim}{\rho}(1-z/L)+\underset{\sim}{K}\cdot\underset{\sim}{b}] \,, \qquad (1)$$

where a is the amplitude of the refractive index fluctuation of the screen, $k=2\pi/\lambda$, where λ is the wavelength of light emitted by the point source, and $\underset{\sim}{K}\cdot\underset{\sim}{b}$ is an arbitrary phase offset. (In passive wind sensing λ varies over a 3 to 1 bandwidth. In this case, the λ inserted into (1) will be the mean wavelength of the background light and photodiode response, which is $\lambda \approx 0.8\mu m$. This can be shown to

---

[1] We measure crosswind by using the slope of the covariance of light intensity fluctuations seen by two horizontally-displaced spatial filters. This method for passive wind sensing has been chosen for the same reasons that make it appropriate for the active system. That is, for a spherical wave source (a scene has many spherical wave sources), an eddy of the same size anywhere along the path contributes to the slope in proportion to its transverse speed. This results in a better average wind measurement. Frequency and time delay methods do not give a true path average in the presence of winds variable in direction or speed along the path.

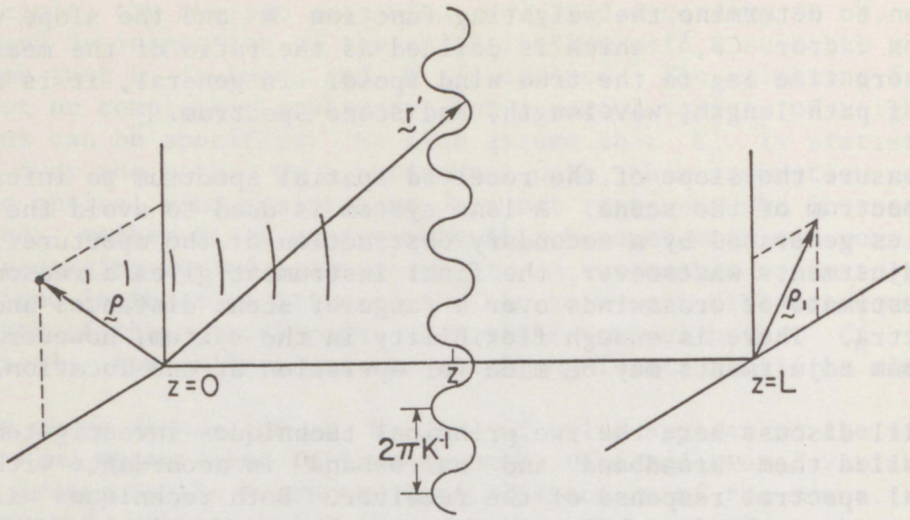

Fig. 2. Geometry of the light source and the receiver. The light at $(\rho,0)$ is perturbed by the turbulent phase screen at z, to produce scintillation in the receiving plane at (ρ,L). The sinusoidal phase screen has a spatial wavenumber K.

produce results that are negligibly different from those of the exact theory that incorporates the appropriately weighted sum of wavelengths.)

The parameter measured by our wind sensing device is not the total field (1) but the normalized amplitude fluctuation dP_a defined by $dP_a = |dE| - 1$. From (1) we have

$$dP_a = k\,adz\,\sin\left[\frac{K^2 z(L-z)}{2kL}\right]\cos\left[\underset{\sim}{K}\cdot\underset{\sim}{\rho}_1(z/L)+\underset{\sim}{K}\cdot\underset{\sim}{\rho}(1-z/L)+\underset{\sim}{K}\cdot\underset{\sim}{b}\right] . \quad (2)$$

If, as we assume in our model, the scene is a sum of spatially incoherent point sources with a distribution $q(\underset{\sim}{\rho})$, we may add the amplitude fluctuations in the following way,

$$dP = k\,adz\,\sin\left[\frac{K^2 z(L-z)}{2kL}\right]\int d^2\underset{\sim}{\rho}\,q(\underset{\sim}{\rho})\cos\left[\underset{\sim}{K}\cdot\underset{\sim}{\rho}_1(z/L)+\underset{\sim}{K}\cdot\underset{\sim}{\rho}(1-z/L)+\underset{\sim}{K}\cdot\underset{\sim}{b}\right] , \quad (3)$$

to calculate the total fluctuations produced by the scene. (This analysis is valid only for a single-scattering, weak turbulence model.) If these fluctuations are observed with a detector of transmittance $t(\underset{\sim}{\rho}_1)$, the detected amplitude variations will take the form

$$dP(\underset{\sim}{r}_1) = k\,adz\,\sin\left[\frac{K^2 z(L-z)}{2kL}\right]\int d^2\underset{\sim}{\rho}_1 t(\underset{\sim}{\rho}_1)\int d^2\underset{\sim}{\rho}\,q(\underset{\sim}{\rho})\cos\left[\underset{\sim}{K}\cdot(\underset{\sim}{\rho}_1+\underset{\sim}{r}_1)(z/L)+\underset{\sim}{K}\cdot\underset{\sim}{\rho}(1-z/L)+\underset{\sim}{K}\cdot\underset{\sim}{b}\right] \quad (4)$$

where $\underset{\sim}{r}_1$ is an arbitrary displacement vector in the plane of $\underset{\sim}{\rho}_1$.

To measure the wind we follow the technique of Lawrence et al. (1972) and use the slope of the covariance of the amplitude fluctuations at zero time lag. Following Lee and Harp (1969), we must first obtain the differential covariance function produced by a single scale-size phase screen at different path positions, i.e.,

$$d\,C_\chi = \langle dP(\underset{\sim}{r}_1)\,dP^*(\underset{\sim}{r}_2)\rangle \tag{5}$$

where the angle brackets indicate an ensemble average and the asterisk implies the complex conjugate. After inserting (4) into (5), we have

$$C_\chi(\underset{\sim}{r}_1,\underset{\sim}{r}_2) = k^2\int_0^L dz_1\int_0^L dz_2\,\sin\left[\frac{K^2 z_1(L-z_1)}{2kL}\right]\sin\left[\frac{K^2 z_2(L-z_2)}{2kL}\right]\int d^2\underset{\sim}{\rho}_1\int d^2\underset{\sim}{\rho}_2 \tag{6}$$

$$\times\, t(\underset{\sim}{\rho}_1)t^*(\underset{\sim}{\rho}_2)\int d^2\underset{\sim}{\rho}'\int d^2\underset{\sim}{\rho}''q(\underset{\sim}{\rho}')q^*(\underset{\sim}{\rho}'')$$

$$\times\,\langle a(\underset{\sim}{K},z_1)\cos[\underset{\sim}{K}\cdot(\underset{\sim}{\rho}_1+\underset{\sim}{r}_1)\cdot(z_1/L)+\underset{\sim}{K}\cdot\underset{\sim}{\rho}'(1-z_1/L)+\underset{\sim}{K}\cdot\underset{\sim}{b}_1]$$

$$a^*(\underset{\sim}{K},z_2)\cos[\underset{\sim}{K}\cdot(\underset{\sim}{\rho}_2+\underset{\sim}{r}_2)(z_2/L)+\underset{\sim}{K}\cdot\underset{\sim}{\rho}''(1-z_2/L)+\underset{\sim}{K}\cdot\underset{\sim}{b}_2]\rangle\ .$$

Equation (6) may be simplified by following the procedure outlined in Appendix I and II of Lee and Harp (1969). This procedure replaces the quantity in the angle brackets with

$$\langle\ \rangle = 2\,F_n(K,z_1-z_2)\cos\left\{\underset{\sim}{K}\cdot[(\underset{\sim}{\rho}_1+\underset{\sim}{r}_1)z_1-(\underset{\sim}{\rho}_2+\underset{\sim}{r}_2)z_2]/L+\underset{\sim}{K}\cdot[\underset{\sim}{\rho}'(1-z_1/L)-\underset{\sim}{\rho}''(1-z_2/L)]\right\}, \tag{7}$$

where F_n is the two-dimensional spectrum of the refractive-index fluctuations. We now substitute (7) into (6), change variables to $2z=z_1+z_2$ and $\xi=z_1-z_2$, perform the ξ integration as outlined in Chapter 7 of Tatarski (1961) for the case $K^2\xi/k\ll 1$, and obtain

$$C_\chi(\underset{\sim}{\rho}) = 4\pi k^2\int_0^L dz\int d^2\underset{\sim}{K}\,\Phi_n(\underset{\sim}{K})\sin^2\left[\frac{K^2 z(L-z)}{2kL}\right]\int d^2\underset{\sim}{\rho}_1\int d^2\underset{\sim}{\rho}_2\,t(\underset{\sim}{\rho}_1)t^*(\underset{\sim}{\rho}_2) \tag{8}$$

$$\int d^2\underset{\sim}{\rho}'\int d^2\underset{\sim}{\rho}''q(\underset{\sim}{\rho}')q^*(\underset{\sim}{\rho}'')\cos[\underset{\sim}{K}\cdot(\underset{\sim}{\rho}_1-\underset{\sim}{\rho}_2+\underset{\sim}{\rho})z/L+\underset{\sim}{K}\cdot(\underset{\sim}{\rho}'-\underset{\sim}{\rho}'')(1-z/L)]$$

where ρ is defined as $\underset{\sim}{\rho}=\underset{\sim}{r}_1-\underset{\sim}{r}_2$. Equation (8) has been generalized to an integral over the full three-dimensional spectrum of refractive turbulence $\phi_n(K)$. (The assumption $K^2\xi/k\ll 1$, as we will see later, requires only that the smallest size eddy in the turbulence spectrum ℓ_0 be much larger than the wavelength. This is a reasonable approximation for the propagation of visible light.)

Further simplification of (8) requires the introduction of the two-dimensional Fourier transform of q and t, i.e.,

$$Q(\underset{\sim}{K}) = \frac{1}{(2\pi)^2}\int d^2\underset{\sim}{\rho}\, q(\underset{\sim}{\rho})e^{-i\underset{\sim}{K}\cdot\underset{\sim}{\rho}} \tag{9}$$

and

$$T(\underset{\sim}{K}) = \frac{1}{(2\pi)^2}\int d^2\underset{\sim}{\rho}\, t(\underset{\sim}{\rho})e^{-i\underset{\sim}{K}\cdot\underset{\sim}{\rho}} \tag{10}$$

and their inverses,

$$q(\underset{\sim}{\rho}) = \int d^2\underset{\sim}{K}\; Q(\underset{\sim}{K})e^{i\underset{\sim}{K}\cdot\underset{\sim}{\rho}} \tag{11}$$

and

$$t(\underset{\sim}{\rho}) = \int d^2\underset{\sim}{K}\; T(\underset{\sim}{K})e^{i\underset{\sim}{K}\cdot\underset{\sim}{\rho}}\ . \tag{12}$$

The first integral that we need to handle in (8) is

$$I_1 = \int d^2\underset{\sim}{\rho}_1 \int d^2\underset{\sim}{\rho}_2\, t(\underset{\sim}{\rho}_1)\; t^*(\underset{\sim}{\rho}_2)\cos[\underset{\sim}{K}\cdot(\underset{\sim}{\rho}_1-\underset{\sim}{\rho}_2+\underset{\sim}{\rho})z/L+\underset{\sim}{K}\cdot(\underset{\sim}{\rho}'-\underset{\sim}{\rho}'')(1-z/L)]\ . \tag{13}$$

If we substitute the appropriate forms of (12) into (13), make the substitution of variables $\underset{\sim}{\rho}_0 = \underset{\sim}{\rho}_1-\underset{\sim}{\rho}_2+\underset{\sim}{\rho}+(\underset{\sim}{\rho}'-\underset{\sim}{\rho}'')(1-z/L)/(z/L)$, and perform the remaining elementary integrals, we eventually obtain for real q, the expression

$$I_1 = (2\pi)^4|T(\underset{\sim}{K}\ z/L)|^2\cos[\underset{\sim}{K}\cdot(\underset{\sim}{\rho}'-\underset{\sim}{\rho}'')(1-z/L)+\underset{\sim}{K}\cdot\underset{\sim}{\rho}z/L]\ . \tag{14}$$

Now we must evaluate

$$I_2 = \int d^2\underset{\sim}{\rho}' \int d^2\underset{\sim}{\rho}''\; q(\underset{\sim}{\rho}')q^*(\underset{\sim}{\rho}'')I_1 \tag{15}$$

which after substitution of (11) and (14) an integrating becomes

$$I_2 = (2\pi)^8|T(\underset{\sim}{K}\ z/L)|^2\ |Q[\underset{\sim}{K}(1-z/L)]|^2\cos(\underset{\sim}{K}\cdot\underset{\sim}{\rho}\ z/L)\ . \tag{16}$$

The factors z/L and $(1-z/L)$, which modify the receiver and transmitter power spectral densities $|T|^2$ and $|Q|^2$, respectively, satisfy the elementary form of reciprocity, i.e., transmitter and receiver spectral densities may be interchanged to give the same result for (8) if $z/L \rightleftarrows 1-z/L$. After (16) is substituted into (8), we obtain

$$C_\chi(\rho) = 4\pi k^2(2\pi)^8\int_0^L dz \int d^2\underset{\sim}{K}\, \sin^2\left[\frac{K^2z(L-z)}{2kL}\right]\cos(\underset{\sim}{K}\cdot\underset{\sim}{\rho}\ z/L)\Phi_n(\underset{\sim}{K})|T(\underset{\sim}{K}\ z/L)|^2|Q[\underset{\sim}{K}(1-z/L)]|^2\ . \tag{17}$$

Equation (17) describes the covariance function of the amplitude fluctuations of an arbitrary incoherent source with spectral density Q^2 observed, through a turbulent medium where refractivity fluctuations have a spectral density Φ_n, with two sets of detectors displaced an amount $\underset{\sim}{\rho}$ and having a spectral density T^2.

To compute the measured time-lagged covariance function, we must replace ρ by $\rho - \underset{\sim}{v}\tau L/z$ (see Clifford 1971) where τ is the time lag, and normalize the expression to $C_\chi(0)$, the variance of the observed signal. This results in

$$C_{\chi N}(\underset{\sim}{\rho},\tau) = N^{-1}\int_0^L dz \int d^2\underset{\sim}{K}\, \sin^2\left[\frac{K^2 z(L-z)}{2kL}\right]\cos[\underset{\sim}{K}\cdot\underset{\sim}{\rho}\, z/L - \underset{\sim}{K}\cdot\underset{\sim}{v}\tau]\Phi_n(\underset{\sim}{K})|T(\underset{\sim}{K}\, z/L)|^2|Q[\underset{\sim}{K}(1-z/L)]|^2 \quad (18)$$

where

$$N = \int_0^L dz \int d^2\underset{\sim}{K}\, \sin^2\left[\frac{K^2 z(L-z)}{2kL}\right] \Phi_n(\underset{\sim}{K})|T|^2|Q|^2 \,. \quad (19)$$

Finally, we determine the slope at zero time lag $m_N = \partial C_{\chi N}/\partial\tau\big|_{\tau=0}$, which equals

$$m_N = N^{-1}\int_0^L dz \int d^2\underset{\sim}{K}\, \sin^2\left[\frac{K^2 z(L-z)}{2kL}\right] (\underset{\sim}{K}\cdot\underset{\sim}{v})\sin[\underset{\sim}{K}\cdot\underset{\sim}{\rho}\, z/L]\Phi_n(\underset{\sim}{K})|T(\underset{\sim}{K}\, z/L)|^2|Q[\underset{\sim}{K}(1-z/L)]|^2. \quad (20)$$

Equation (20) is the general expression of the passive wind sensing formula. We will want to particularize the form of (20) in the next sections to study some practical systems.

2.1 Broadband Wind Sensing

In the case where the receiver configuration is two circular apertures of diameter D, $|T|^2$ is simply a low-pass filter function,

$$|T(\underset{\sim}{K}\, z/L)|^2 \sim \left[\frac{2J_1\left(\frac{KDz}{2L}\right)}{\left(\frac{KDz}{2L}\right)}\right]^2 \quad (21)$$

We must now consider the forms of the two other spectral quantities in (20): the refractive-index spectral density Φ_n and the scene spectrum $|Q|^2$.

The most commonly accepted form of the spectrum of refractive turbulence is that due to Kolmogorov (1941). He postulated from dimensional analysis arguments that, within the so-called inertial subrange, defined by $L_0^{-1} << K << \ell_0^{-1}$ where ℓ_0 and L_0 are the inner and outer scales of turbulence, respectively, the spectral density of the refractive-index fluctuations should have the form

$$\Phi_n(K) = 0.033\, C_n^2(z)K^{-11/3} \,. \quad (22)$$

We will use this spectrum throughout this report. We have chosen to analyse our experimental results in terms of power law spectra for the

scene. Of course we eventually hope to remove this restriction and study our results based upon more realistic measured spectra. In preliminary measurements of scene spectra we have found that power law spectra of the form

$$|Q[\underset{\sim}{K}(1-z/L)]|^2 = A[K(1-z/L)]^{-\alpha} , \tag{23}$$

with $0<\alpha<3$, reasonably represent the two-dimensional spectra of typical scenes.

With (21), (22), and (23) substituted into (20), we can change d^2K to polar coordinates $KdKd\theta$ and integrate over angle. With this accomplished, we obtain

$$m_N = N_1^{-1}\int_0^L dz \; \frac{C_n^2(z)v(z)}{(1-z/L)^{\alpha}} \int_0^{\infty} dK \; K^{-5/3-\alpha} \sin^2\left[\frac{K^2z(L-z)}{2kL}\right] J_1(K\rho z/L)\left[\frac{2J_1\left(\frac{KDz}{2L}\right)}{\left(\frac{KDz}{2L}\right)}\right]^2 , \tag{24}$$

where J_1 is the first order Bessel function of the first kind and the normalization factor N_1 is given by

$$N_1 = \int_0^L dz \; \frac{C_n^2(z)}{(1-z/L)^{\alpha}} \int_0^{\infty} dK \; K^{-8/3-\alpha} \sin^2\left[\frac{K^2z(L-z)}{2kL}\right] \left[\frac{2J_1\left(\frac{KDz}{2L}\right)}{\left(\frac{KDz}{2L}\right)}\right]^2 . \tag{25}$$

In obtaining (24), we have assumed that the dominant wind component is parallel to the spacing of the two detectors. This is a reasonable assumption for our near-ground, horizontal paths. For convenience in plotting curves, we change variables to $u=z/L$, $y=K\sqrt{\lambda L}$, $D_n=D/\sqrt{\lambda L}$, and $\rho_n = \rho/\sqrt{\lambda L}$; and (24) becomes

$$m_N = (\lambda L)^{-1/2}\int_0^1 du \; C_n^2(u)v(u)W(u)/\left[\int_0^1 du \; C_n^2(u)W'(u)\right] \tag{26}$$

where $W(u)$ is given by

$$W(u) = (1-u)^{-\alpha}\int_0^{\infty} dy \; \sin^2\left[\frac{y^2u(1-u)}{4\pi}\right] y^{-8/3-\alpha} J_1(y\,\rho_n u)\left[\frac{2J_1(yD_nu/2)}{(yD_nu/2)}\right]^2 \tag{27}$$

and

$$W'(u) = (1-u)^{-\alpha}\int_0^{\infty} dy \; \sin^2\left[\frac{y^2u(1-u)}{4\pi}\right] y^{-8/3-\alpha}\left[\frac{2J_1(yD_nu/2)}{(yD_nu/2)}\right]^2 . \tag{28}$$

If we assume that C_n^2 is statistically uniform along the path, then $W(u)$ becomes proportional to the wind weighting function.

Some representative results for $W(u)$ are plotted in figures 3, 4, and 5. Each curve is a plot of $W(u)$ for two tangent apertures ($\rho_n = D_n$) of diameter D, normalized to a Fresnel zone $\sqrt{\lambda L}$, with λ the mid-bandwidth wavelength. In all three figures, the slope-wind calibration factor CF is proportional to the areas under the curves. The scene is on the left and the receivers on the right. Figure 3 shows the result for white noise, $\alpha=0$. Interestingly, it is also the same weighting as the familiar case for a point light source. Figure 4 is the result for $\alpha=1$. Note how the reduction of small spatial sizes in the light source moves the weighting functions toward the receiver. However, by enlarging the receiver (increasing ρ_n) these functions may be shifted back somewhat toward the light source. The area under these curves is proportional to the slope-wind relationship. In figure 5, some receiver configurations are plotted for a spatial spectrum of slope $\alpha=2$. (In figure 5 we have assumed an "outer scale" for the scene spectrum. This is the reason that the weighting functions all go to zero at the receiver instead of the finite constant indicated by (27).)

Although the weighting functions obtained for the two-aperture (broadband) case are attractive, practical difficulties are encountered in an actual system. Temporal changes in illumination of the scene due to movement or AC lights are not even partially cancelled out, and lead to large errors even though the variation is of the order of 10^{-4} the light level of the entire scene. In addition, the broadband signal-to-noise level is not as high as can be obtained in a narrower band system.

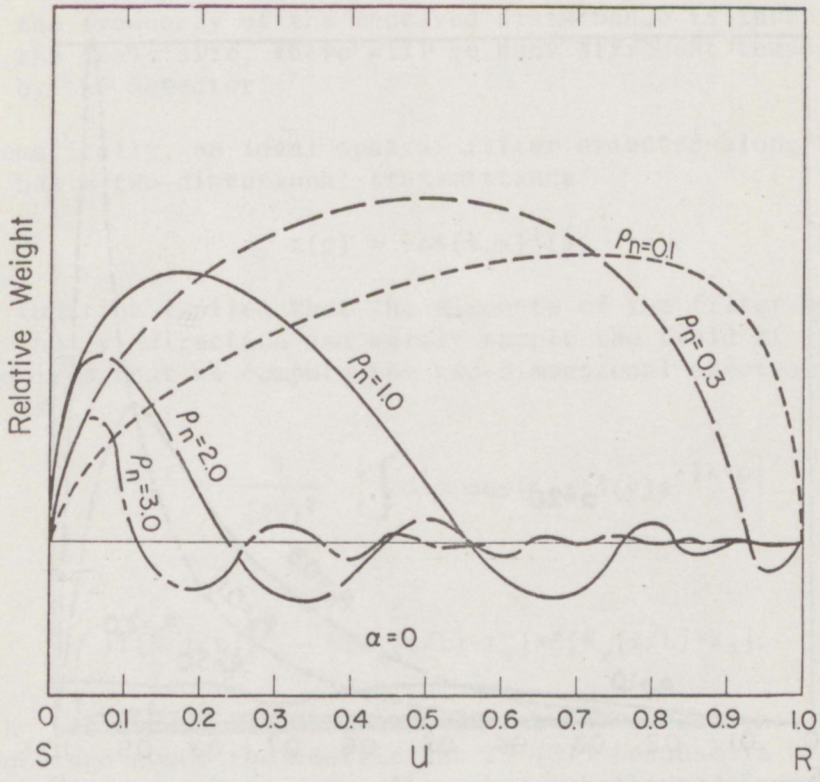

Fig. 3. Wind weighting functions for a scene with a spectral slope $\alpha=0$.

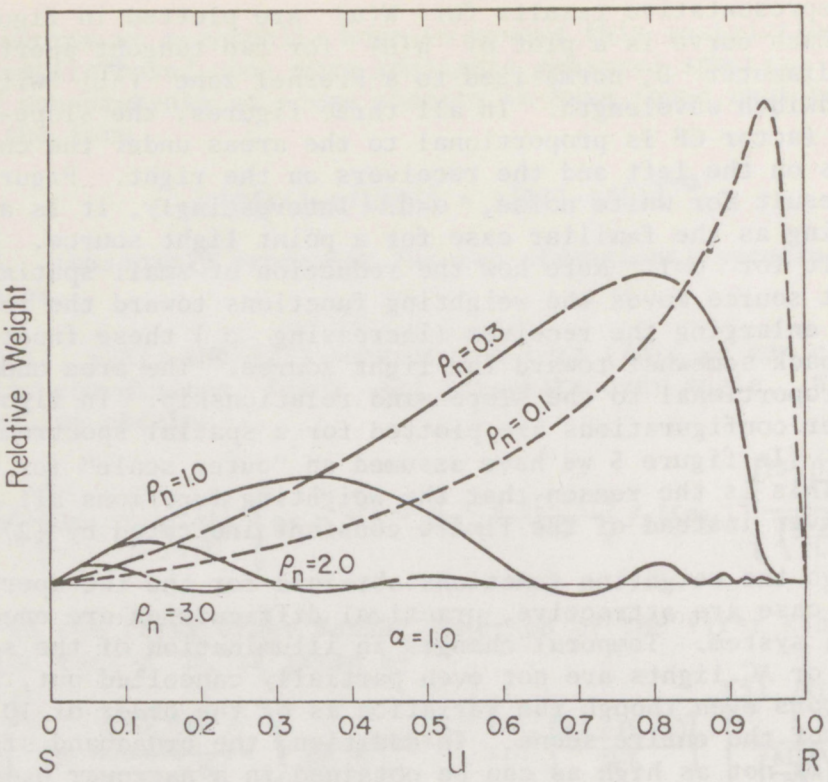

Fig. 4. Wind weighting functions for a scene with a spectral slope α=1.

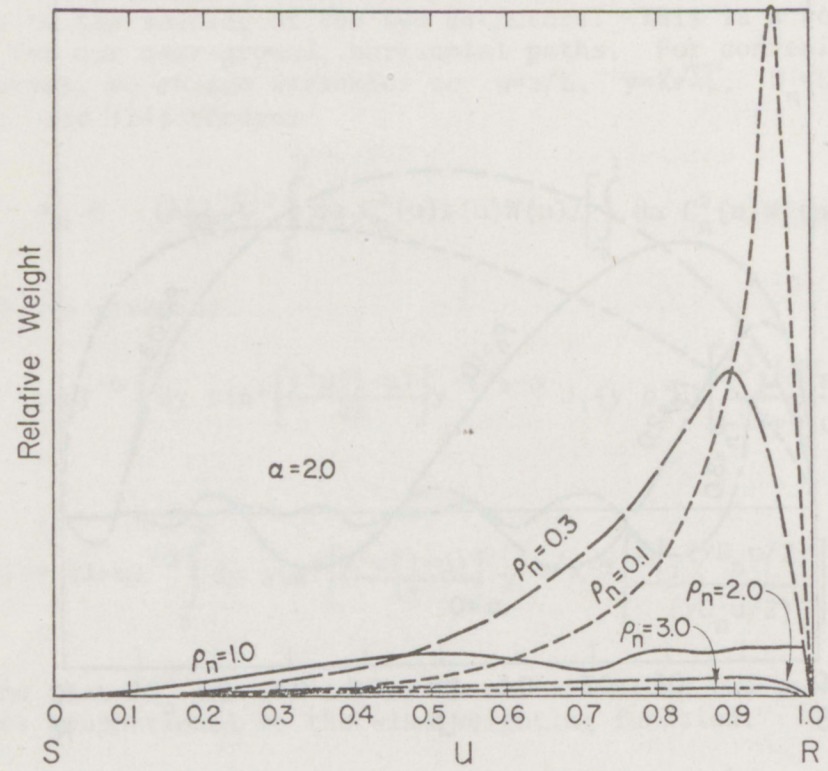

Fig. 5. Wind weighting functions for a scene with a spectral slope α=2.

Some of these problems could be remedied by taking the difference of the signals in two widely spaced aperture pairs. Continuing in this direction leads to the analysis of the performance of narrowband spatial arrays for passive wind sensing.

2.2 Narrowband Wind Sensing

Because of the difficulties in effectively implementing the broadband system, as mentioned in the last section, we have chosen a narrowband approach. In this technique we spatially filter the received signal along one dimension parallel to the component of wind that is transverse to the beam. Using an array of photodiodes, we synthesize an effective sinusoidal filter that observes a single spatial frequency in the horizontal direction. By using two of these devices, separated by a phase lag of ϕ degrees in terms of the fundamental wavelength $2\pi/K_0$ of the filter, we measure the speed of advection of this wavelength disturbance at the reciever. Filtering does not produce a single sinusoidal disturbance in time because of the many different path positions to which this filter is sensitive. For example, each point source of light in the scene causes a geometric magnification of the turbulent eddies that each source illuminates along the propagation path (see Lawrence et al. 1972). This makes the spatial filter sensitive to spatial scale sizes of refractive turbulence that are proportional to the distance from the scene. Since the wind profile is not uniform and since the frequency of the received disturbance is inversely proportional to the scale size, there will be many different temporal frequencies collected by the detector.

Mathematically, an ideal spatial filter oriented along the x direction has a two-dimensional transmittance

$$t(\underset{\sim}{\rho}) = \cos(K_0 x)\delta(y) \tag{29}$$

The delta function implies that the elements of the filter have zero extent in the y direction and merely sample the field at $y=0$. The theory requires that we compute the two-dimensional spectral density of t, which is

$$|T|^2 = \frac{1}{(2\pi)^2} \left| \int d^2\underset{\sim}{\rho}\, \cos(K_0 x)\delta(y) e^{-i\underset{\sim}{K}\cdot\underset{\sim}{\rho}} \right|^2 \tag{30}$$

or

$$|T(\underset{\sim}{K}\, z/L)|^2 \sim \delta[K_x(z/L)-K_0]+\delta[K_x(z/L)+K_0]. \tag{31}$$

In (31) K_x is the component of $\underset{\sim}{K}$ in the x direction. [We need not be concerned about the coefficient in (31) because it will drop out of the normalized covariance function when substituted into (20).]

To complete the calculation, we substitute (31), (22), and (23) into (19) and (20); let $K_1 = K_y z/L$; perform the K_x integration to obtain

$$m_N = N_1^{-1} K_0 \sin\phi \int_0^L dz \; \frac{C_n^2(z) v(z) (z/L)^{2/3+\alpha}}{(1-z/L)^{\alpha}} \int_{-\infty}^{\infty} dK_1 \sin^2[(K_0^2+K_1^2)(L/z-1)L/(2k)](K_0^2+K_1^2)^{-11/6-\alpha/2} \tag{32}$$

and

$$N_1 = \int_0^L dz \; \frac{C_n^2(z) (z/L)^{5/3+\alpha}}{(1-z/L)^{\alpha}} \int_{-\infty}^{\infty} dK_1 \sin^2[(K_0^2+K_1^2)(L/z-1)L/(2k)](K_0^2+K_1^2)^{-11/6-\alpha/2} . \tag{33}$$

In (32) we have written the separation ρ in terms of the phase-angle $\phi = K_0 \rho$. Also, we have assumed that $\underset{\sim}{\rho} \| \underset{\sim}{v} \| \hat{\underset{\sim}{x}}$ where $\hat{\underset{\sim}{x}}$ is an x-directed unit vector. To put (32) and (33) in a more useful form for computing, we let $u = z/L$, $t = K_1 \sqrt{\lambda L}$, and $t_0 = K_0 \sqrt{\lambda L}$ where, as before, λ is the wavelength at mid-bandwidth, and we obtain

$$m_N = t_0 \sin\phi \, (\lambda L)^{-1/2} \int_0^1 du \; C_n^2(u) v(u) W_f(u) \Big/ \left[\int_0^1 du \; C_n^2(u) W_f'(u) \right] \tag{34}$$

with

$$W_f(u) = \frac{u^{2/3+\alpha}}{(1-u)^{\alpha}} \int_0^{\infty} dt \; \sin^2[(t_0^2+t_1^2)(1/u-1)/(4\pi)](t_0^2+t_1^2)^{-11/6-\alpha/2} \tag{35}$$

and $W_f'(u) = u W_f(u)$. As before, when C_n^2 is uniform along the path, $W_f(u)$ is proportional to the wind weighting function.

There are two important characteristics of (34) and (35) that must be considered in the design of the passive wind sensor. The first is the wind weighting function $W_f(u)$ and the second is the calibration factor CF defined by

$$CF \equiv m_N/\bar{v} = t_0 \sin\phi \, (\lambda L)^{-1/2} \int_0^1 du \; W_f(u) \Big/ \left[\int_0^1 du \; u W_f(u) \right] . \tag{36}$$

This quantity, which is defined only when C_n^2 is uniform along the path, is the proportionality constant between the slope and the average wind.

Figures 6 through 9 show the behavior of the wind weighting function and CF as a function of the spectral power law for a scene as a function of normalized wavelength of the receiving spatial filter $d_n = 2\pi/t_0 = 2\pi/(K_0 \sqrt{\lambda L})$ for $\phi = \pi/2$. Note that, for a fixed filter wavelength, as the scene

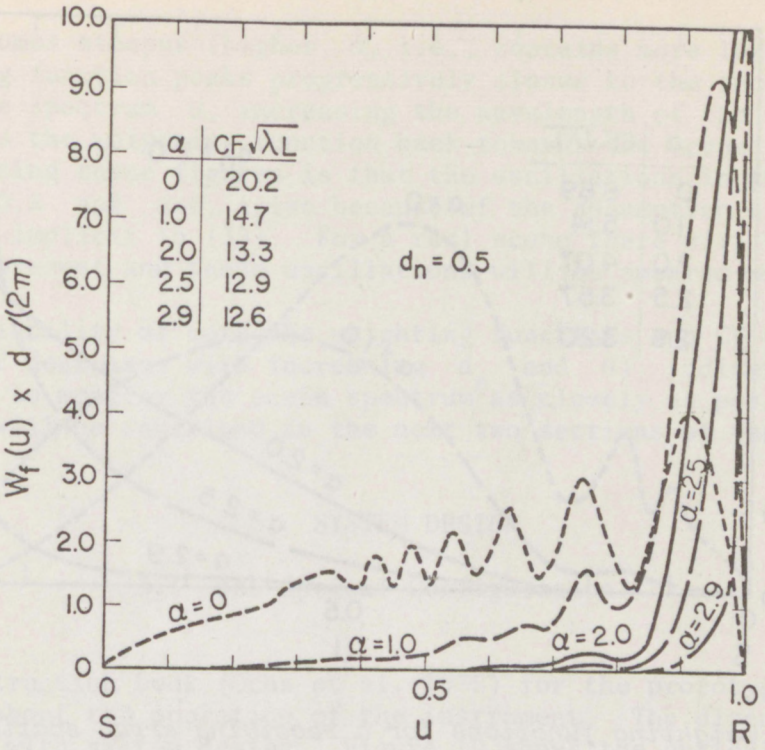

Fig. 6. Wind weighting functions for a receiving array spatial wavelength d_n=0.5. ($d=d_n(\lambda L)^{\frac{1}{2}}$).

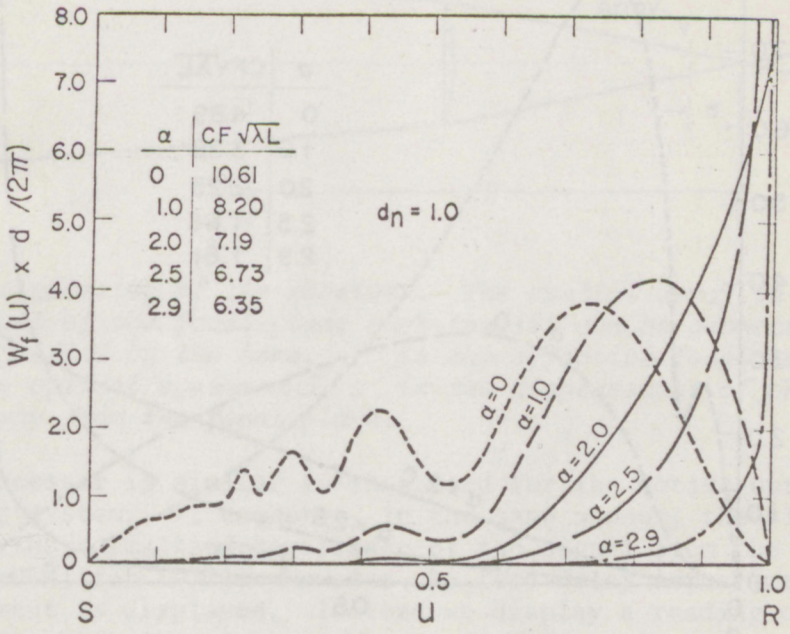

Fig. 7. Wind weighting functions for a receiving array spatial wavelength d_n=1.

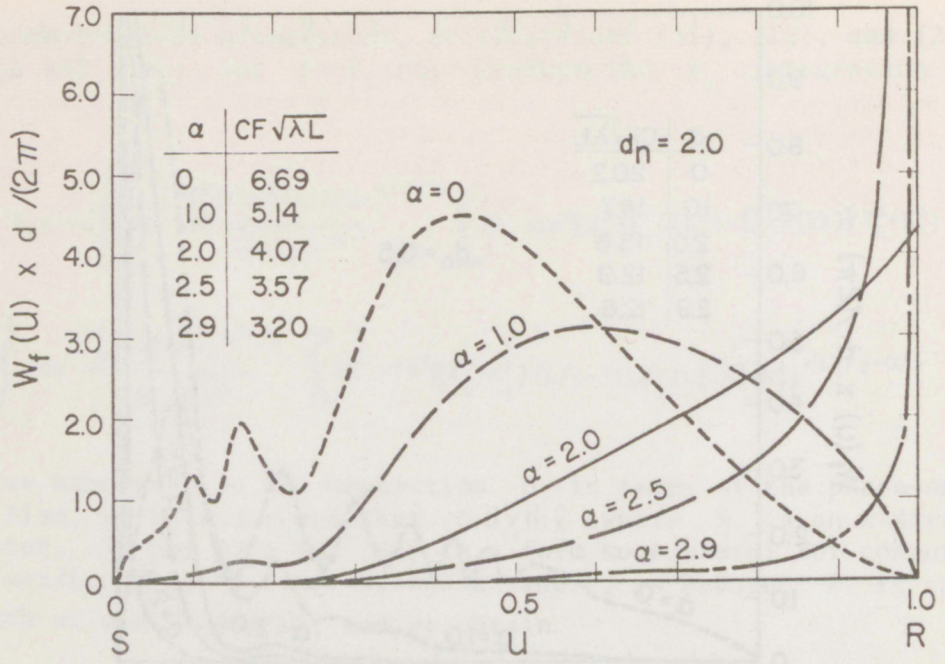

Fig. 8. Wind weighting functions for a receiving array spatial wavelength d_n=2.

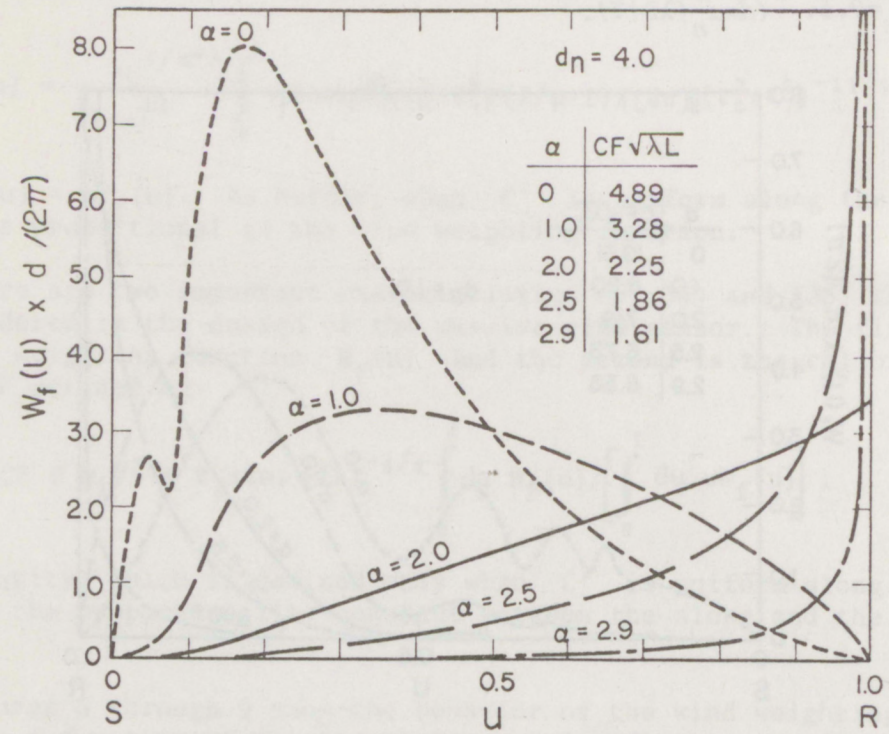

Fig. 9. Wind weighting functions for a receiving array spatial wavelength d_n=4.

spectrum becomes steeper (higher α, i.e., contains more low frequencies), the weighting function peaks progressively closer to the receiver. For a fixed scene spectrum α, increasing the wavelength of the filter tends to bias the weighting function back towards the scene. One caution in using these figures is that the oscillations in the curves, say for $d_n=0.5$ and $\alpha=0$, arise because of the assumption of monochromaticity implicit in (35). For a real scene there will be many frequencies present and these oscillations will be smeared out.

The variability of both the weighting functions and CF with α (note that CF decreases with increasing d_n and α) indicates that it is desirable to monitor the scene spectrum as closely as possible. This effect will be described in the next two sections of this report.

3. SYSTEM DESIGN

3.1 The Optical Configuration

The instruction book (Ochs et al. 1975) for the prototype contains information about the operation of the instrument. The discussion here is concerned with system design. Figure 10 shows the optical design of the receiver and figure 11 is a block diagram of the signal processor.

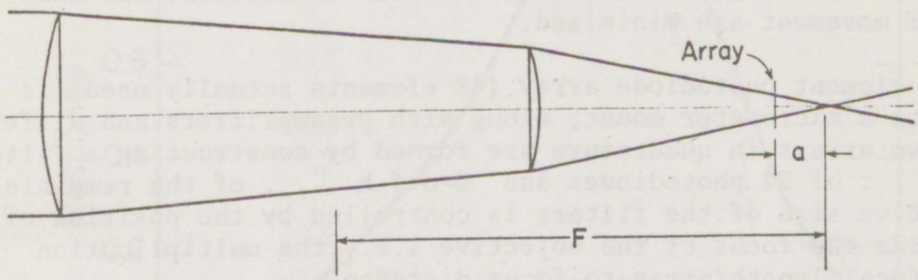

Fig. 10. The geometry of the receiver. The spatial array is placed in front of the focal plane such that it can be geometrically magnified by the lens. F is the effective focal length of the optical system and a is the displacement of photodiode array from the focal plane.

The signal processor is similar to that used for the active optical wind measuring system. It computes, in the same manner, the slope at zero delay of the normalized covariance of the signal from the photodiode array (Ochs and Miller 1972). However, no zero-delay normalized covariance measurement is displayed. Instead we display a reading of the power in dB of the fluctuating component of the signal at one spatial wavelength.

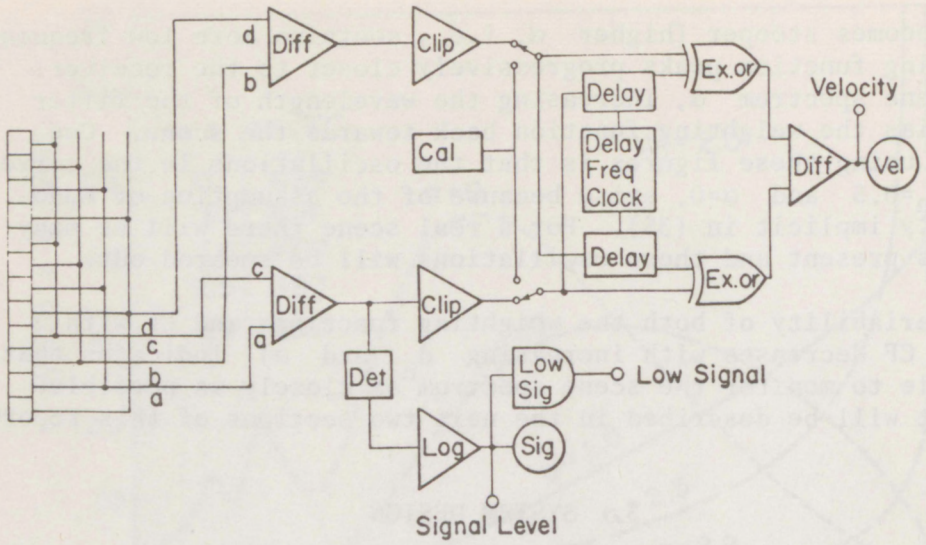

Fig. 11. Block diagram of the system.

In figure 10, a combination of 12.2 cm and 7.5 cm diameter lenses is used to form an objective having a focal ratio of 2.39 and a focal length of 30.4 cm. A low focal ratio is necessary to obtain high irradiance and thus relatively high signal fluctuation after removal of the mean. It also helps, in a less obvious way, to assure that angular fluctuations have little contribution to the measurement and that effects of movement are minimized.

A 50-element photodiode array (48 elements actually used) is attached to a micrometer mount, along with preamplifiers and differencing units. Two arrays in quadrature are formed by constructing a filter a-c+e-g . . . of 24 photodiodes and b-d+f-h . . . of the remaining 24. The effective size of the filters is controlled by the position of the array inside the focus of the objective i.e., the multiplication factor = focal length/array-to-focus distance.

As far as the multiplication factor is concerned, there is no difference whether the array is inside or outside of the infinity focus of the lens. There is, however, a difference in the wind weighting function because of different angular effects. For the inside-focus position, the effective aperture is that projected on and located at the real objective. For the same array distance outside of focus, the effective aperture is the same size but is located at the image plane of the array out in space. The resulting weighting function from this image plane to the scene would be that for an aperture of this size at this location. We use the inside focus position for the array in our instrument, since this configuration is less sensitive to motion in the scene.

From figure 10, the array amplification factor is F/a where F is the effective focal length of the lens system and a is the distance inside focus. The effective spatial wavelength in the optical system, in units of Fresnel zones, is $d_n = Fs/(a\sqrt{\lambda L})$, where s is the actual wavelength of the photodiode array. In the instrument, $s = 8.00 \times 10^{-4}$ m and $F = 0.304$ m so the micrometer setting a in meters is

$$a = Fs/(d_n\sqrt{\lambda L}) = 2.43 \times 10^{-4}/d \qquad (37)$$

for a given spatial wavelength.

A spatial wavelength having a suitable wind weighting function may be selected from figures 6 through 9. The spatial wavelengths in these plots are normalized in terms of Fresnel zones $\sqrt{\lambda L}$, where L is the distance from the scene to the receiver and $\lambda = 0.8 \times 10^{-6}$ m is the mean wavelength of the observed illumination, i.e., the product of the spectrum of ambient daylight and the photodiode spectral response. The actual wavelength response is shown in figure 12. The broad range of wavelengths is beneficial in that it tends to smooth out the small details in some of the weighting functions.

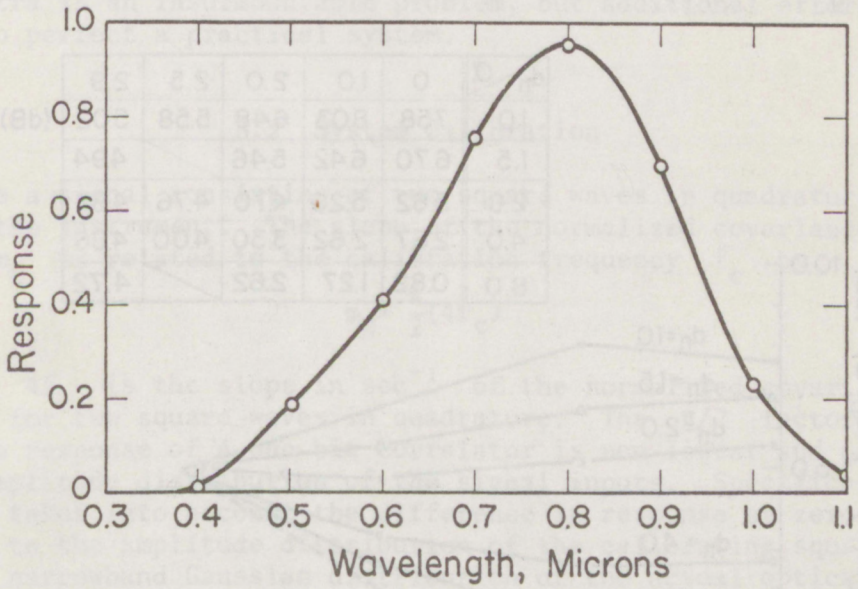

Fig. 12. Spectral response of daylight-photodiode combination.

Most scenes have a two-dimensional spatial spectrum that, in the region of interest, is approximately $K^{-2.5}$; i.e., $\alpha = 2.5$. If bright lights or reflective glints are present in the scene, these will predominate and α will be nearly zero (i.e. the flat spectrum one expects from a point light source). Generally, then, the scene may be considered to have a spectrum of one or the other or these extremes, and the weighting function and calibration can be estimated accordingly.

In principle, a measurement of the spatial spectrum of the scene may be derived from the signal meter on the instrument. If we measure the variances of the irradiance (or amplitude) scintillations for two different spatial wavelengths d_n and d_n', then the ratio $\sigma_\chi^2(d_n)/\sigma_\chi^2(d_n')$ is a function of the scene spectrum, although somewhat contaminated by the intervening turbulence. The variance σ_χ^2 can be obtained by

$$\sigma_\chi^2(d_n) \sim \int_0^1 du\ C_n^2(u) u W_f(u, d_n) \tag{38}$$

where $W_f(u)$ is defined by (35). The proportionality constant in (38) is not important since it will be cancelled when we take the ratio of the variances. If we set $d_n'=d_n/2$ and again assume that $C_n^2(u)$ is uniform along the path, the ratio $\sigma_\chi^2(d_n)/\sigma_\chi^2(d_n/2)$, plotted against the exponent of the scene spectrum α, varies as shown in figure 13 for different d_n. Although for d_n between 2 and 4 the ratio is not sensitive to α, for either larger or smaller d_n the difference between $\alpha=0$ and $\alpha=2.5$ is detectable. Once α is known, the weighting function and the slope-wind relationship can be determined from figures 6 through 9.

d_n \ α	0	1.0	2.0	2.5	2.9
1.0	7.58	8.03	6.48	5.58	5.02
1.5	6.70	6.42	5.46		4.94
2.0	5.62	5.20	4.70	4.76	4.87
4.0	2.67	2.62	3.30	4.00	4.86
8.0	0.82	1.27	2.62		4.72

(dB)

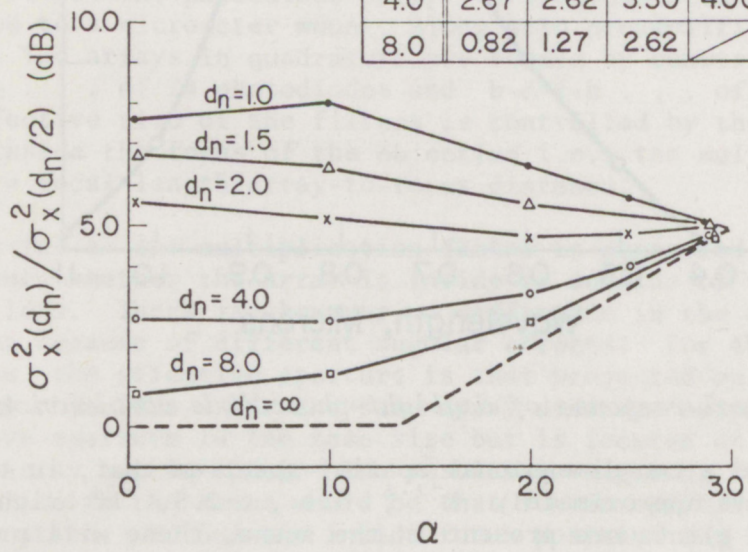

Fig. 13. The ratio of the variances detected by two spatial arrays with the spatial wavelengths d_n and $d_n/2$ vs the spatial spectral slope α of the scene.

We were unable to obtain satisfactory experimental verification of this technique for remotely measuring the scene spectrum. Actually, three other systems for remotely measuring spatial scene spectra were also experimentally evaluated. The first deduced the spectrum from a measurement of the normalized covariance at zero delay. This measurement suffered from the same difficulties as that of the two-aperture passive wind measurement mentioned at the end of 2.1.

By connecting a photodiode array to observe the signal power simultaneously at two spatial wavelengths, we attempted to measure the slope of the received spatial spectrum. Again the result seemed too contaminated by noise for satisfactory use.

In principle, a direct measurement of the slope of the scene spatial spectrum could be made by placing arrays sensitive to two wavelengths in the receiver focal plane. Contrary to the previous methods, this measurement is affected by atmospheric turbulence. However, the main difficulty encountered in this arrangement appeared to be insufficient sampling of the scene, with the arrays stationary in the image plane. We do not feel that the satisfactory measurement of scene spectra is an insurmountable problem, but additional effort is required to perfect a practical system.

3.2 System Calibration

We use a signal consisting of two square waves in quadrature to calibrate the instrument. The slope of the normalized covariance function m_N is related to the calibration frequency f_c by

$$m_N = \frac{\pi}{2}(4f_c) \tag{39}$$

The factor $4f_c$ is the slope in $\sec^{-1}$ of the normalized covariance at zero delay for two square waves in quadrature. The $\pi/2$ factor arises because the response of a one-bit correlator is non-linear and depends upon the amplitude distribution of the signal inputs. Specifically, the factor takes into account the difference in response at zero covariance to the amplitude distribution of the calibrating square wave and to the narrowband Gaussian distribution of the actual optical signal.

As previously noted, the area under the weighting functions of figures 6 through 9 is the calibration factor CF. It is related to the actual covariance slope m_N by

$$m_N = (CF)v. \tag{40}$$

Using (39) and (40) we may obtain the calibration frequency[2]

$$f_c = \frac{|m_N|}{2\pi} = \frac{|CF\ v|}{2\pi} \qquad (41)$$

In concept, the instrument could be designed to maintain its calibration automatically and to maintain approximately the desired weighting function, with distance to the scene being the only external input required. The spatial spectrum of the scene could be continuously monitored and the instrument itself could perform the calibration, based upon the relationships developed in this paper.

There are modes of operation, assuming a typical scene spectrum, for which the calibration of the instrument remains nearly independent of scene distance. In figures 14 through 18 weighting functions have been replotted to illustrate the performance of the instrument when the array is set and left at a given spatial size d, and the scene distance L is allowed to vary. The weighting functions are plotted and CF determined for five scene spectral slopes, α=0, 1, 2, 2.5, and 2.9. (For the typical scene, α would range between 2 and 2.5).

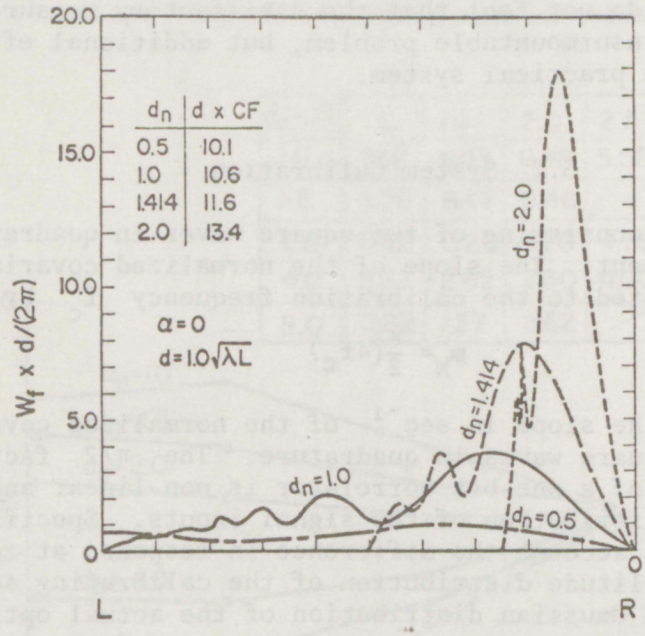

Fig. 14. Wind weighting function for a scene with a spatial spectral slope α=0.

[2]As an example of the use of these calculations, assume a scene 500 m distant with α=2. Assume that the weighting function for the case d_n=1 is the one desired. From figure 7 we see for this particular set of parameters that the weighting function labeled α=2.0 applies to this case and also that CF= $7.19/\sqrt{\lambda L}$. Using the mid-bandwidth wavelength $\lambda = 0.8\times10^{-6}$ and L=500 m, we obtain a calibration factor CF= 360. The micrometer setting to achieve d_n=1 is found from (37) to be a=1.22 cm. The calibration frequency for 10 m/sec full scale from (41) is f_c=573 Hz.

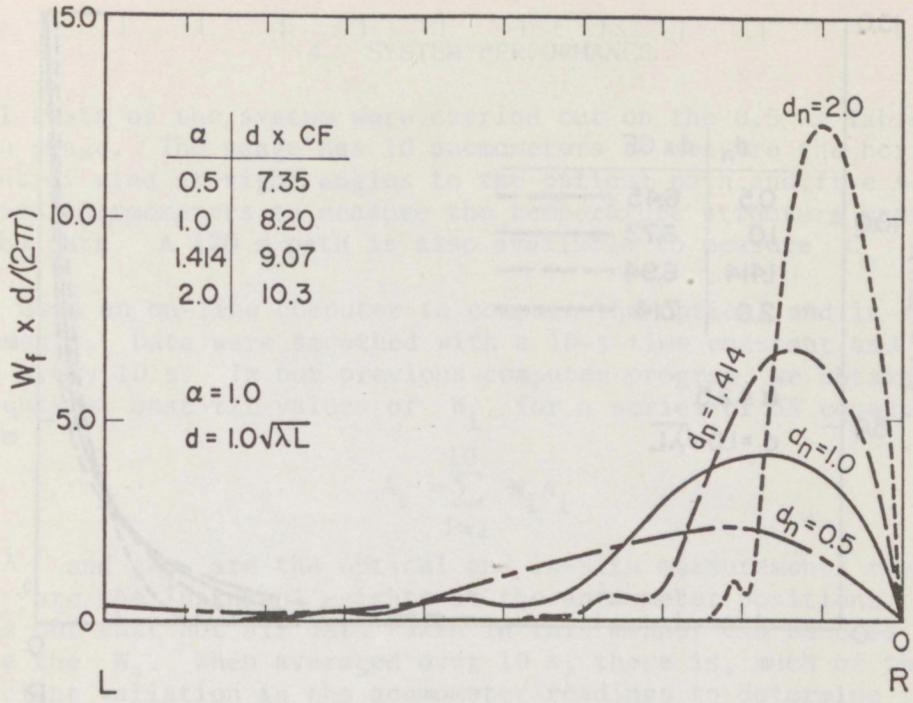

Fig. 15. Wind weighting function for a scene with a spatial spectral slope α=1.

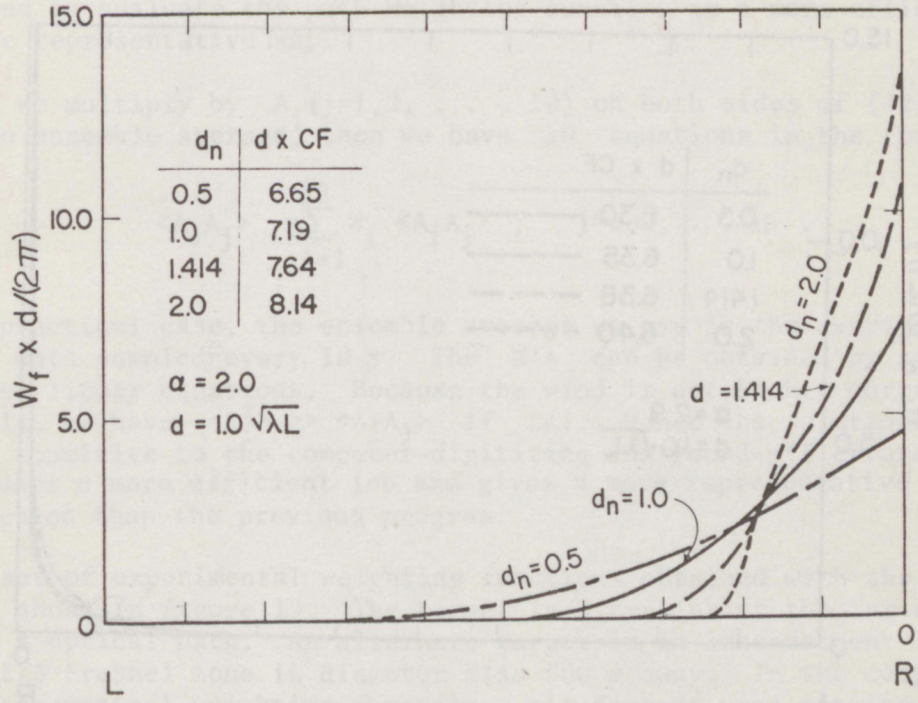

Fig. 16. Wind weighting function for a scene with a spatial spectral slope α=2.

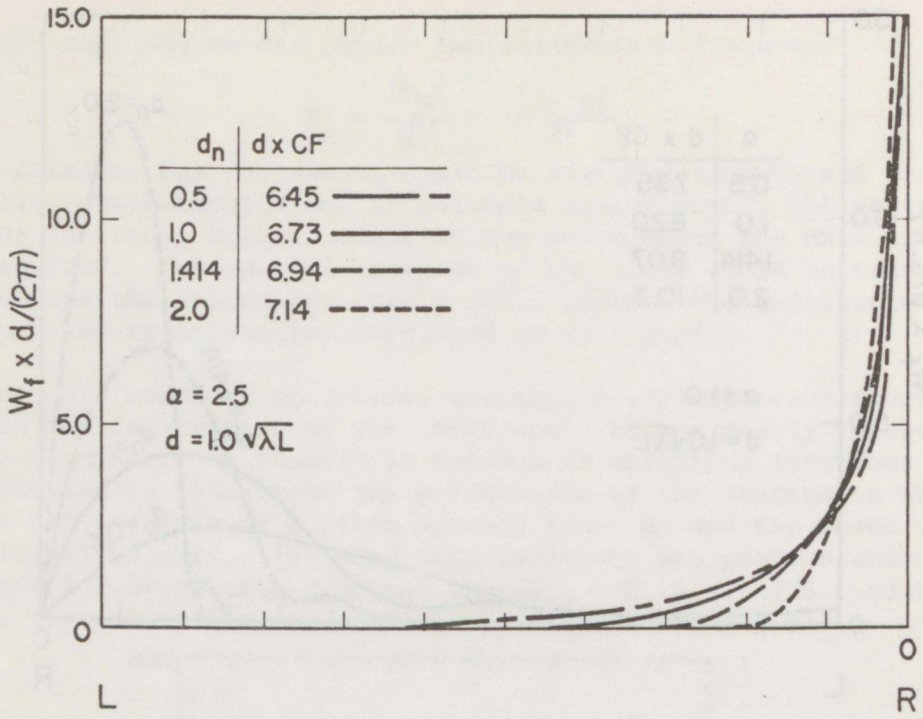

Fig. 17. Wind weighting function for a scene with a spatial spectral slope α=2.5.

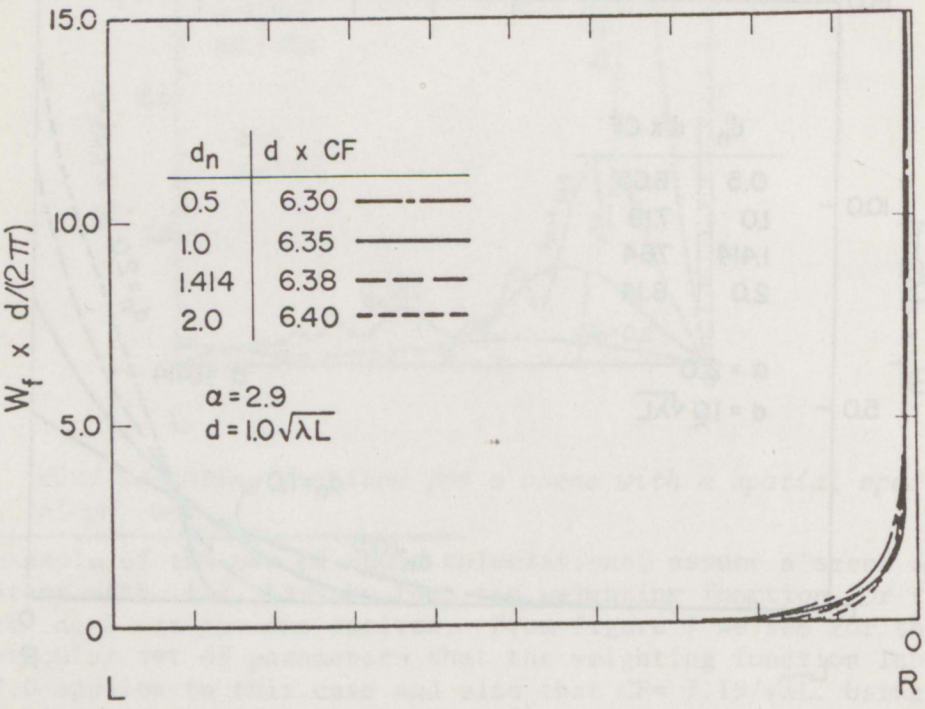

Fig. 18. Wind weighting function for a scene with a spatial spectral slope α=2.9.

4. SYSTEM PERFORMANCE

All tests of the system were carried out on the 0.5 km Table Mountain range. The range has 10 anemometers to measure the horizontal component of wind at right angles to the optical path and five sets of high-speed thermometers to measure the temperature structure constant along the path. A 170 m path is also available to measure C_n optically.

We used an on-line computer to compare the optical and in-situ measurements. Data were smoothed with a 10-s time constant and then sampled every 10 s. In our previous computer program, we obtained the least-squares, best-fit values of W_i for a series of 38 equations of the form

$$A_0 = \sum_{i=1}^{10} W_i A_i \tag{42}$$

where A_0 and A_i are the optical and in-situ measurements respectively and W_i are the (unknown) weights at the anemometer positions. However, it turns out that not all data taken in this manner can be used to evaluate the W_i. When averaged over 10 s, there is, much of the time, insufficient variation in the anemometer readings to determine W_i. The 10 s averaging period is necessary so that the point measurements are more nearly like the 40-m space-average that they are supposed to represent. Because of this disadvantage, a new technique has been developed to evaluate the path-weighting function in a more efficient and more representative way.

If we multiply by A_j (j=1,2, . . . 10) on both sides of (42) and take the ensemble average, then we have 10 equations in the form

$$\langle A_0 A_j \rangle = \sum_{i=1}^{10} W_i \langle A_i A_j \rangle \; ; \quad j=1,2, \ldots 10 \; . \tag{43}$$

In the practical case, the ensemble average we use is the average of 88 sets of data sampled every 10 s. The W's can be obtained by solving these ten linear equations. Because the wind is not highly correlated spatially, we have $\langle A_i^2 \rangle >> \langle A_i A_j \rangle$ if $i \neq j$. Hence the solutions of W are not sensitive to the computer-digitizing and round-off errors. This method does a more efficient job and gives a more representative weighting function than the previous program.

A set of experimental weighting functions obtained with the instrument is shown in figure 19. The target is a trailer at the far end of the 500 m optical path. An alternate target is an incandescent light source 1/3 Fresnel zone in diameter also 500 m away. In the computation of the theoretical weighting functions, all factors were retained so that the area under these curves is the calibration factor, and this factor can be compared with the experimental results (Table 1).

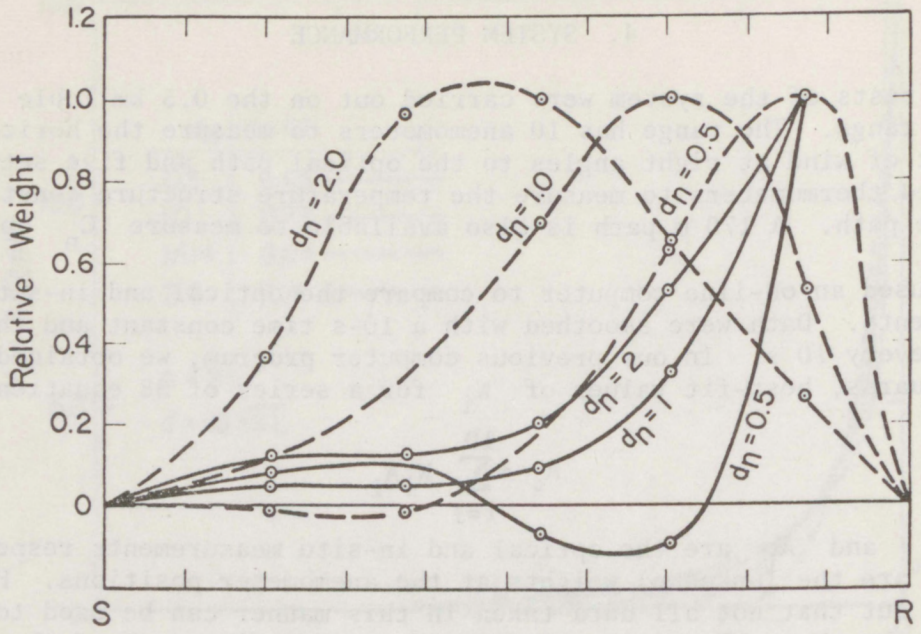

Fig. 19. Experimental wind weighting functions for an incandescent light source (dashed curves), and a trailer in bright sunlight (solid curves). The functions have been normalized by setting the largest ordinate of each curve to 1.

Table 1. Theoretical and Experimental Calibration Factors.

d_n	theoretical		experimental	
	$CF\sqrt{\lambda L}$ $\alpha=0$	$CF\sqrt{\lambda L}$ $\alpha=2.5$	$CF\sqrt{\lambda L}$ light	$CF\sqrt{\lambda L}$ trailer
0.5	20.2	12.9	15.3	7.9
1	10.6	6.9	4.3	3.4
2	6.7	3.6	1.8	1.3

Though the general form of the weighting functions is as predicted, the calibration factors are not. Best agreement is obtained for d_n small, when the array is farthest from the focus. This may indicate that angular-fluctuation effects, which would be more pronounced near the focus, significantly affect the measurement. Some approximations are present in the spectral description of the scene and the assumption of narrowband Gaussian statistics for the fluctuating optical signal.

There are also inner-scale effects on this short a path which have not been taken into account. The experimental study using the prototype instrument indicates CF values approximately 0.6 that of the theoretical results so these values should be used in the calibration of the prototype.

By averaging the outputs of the five anemometers on half of the 500-m path nearest the instrument, we have the comparison shown in figure 20. The agreement over short time intervals would presumably be even better had anemometers been weighted according to the weighting function of the optical instrument.

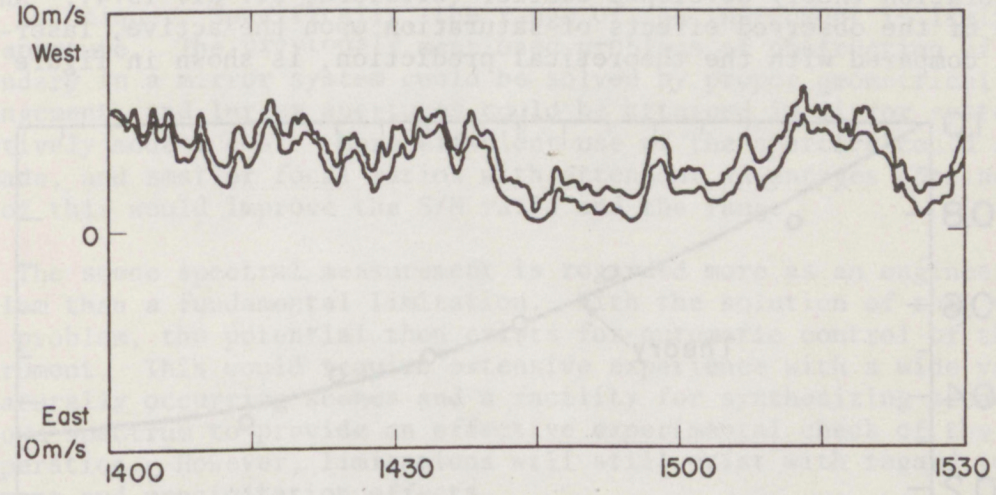

Fig. 20. A comparison of the transverse wind speed measured by the optical system (upper trace) with the average of wind speeds measured by five anemometers equally spaced on half of the 500-m path nearest the instrument. The gain of the optical system was increased to displace the curves.

A number of additional factors arise in an actual instrument. First of all, the signal-to-noise problem is severe. It is hard to specify S/N in a meaningful way since the fractional modulation of the irradiance is a function of C_n^2, path length, scene spectrum irradiance, and photodiode array setting. On a sunny day with a typical scene and the optical path several meters above the ground, the fractional modulation of the irradiance is approximately 10^{-3}. As the noise level is about 5×10^{-5} that of the ambient illumination, there may be times on a cloudy day with low C_n^2 when there is insufficient S/N for the system to operate.

The instrument and the scene should be stationary, although the system is designed to minimize effects of movement. The differencing circuits remove overload symmetrically around the mean to minimize the effects of large transients on the low-frequency cutoff filters. In

addition, the inside-focus position for array amplification is used, so that the scene image is farther out of focus than would be the case for the outside-focus location. Again, the seriousness of these effects depends upon the scintillation level. White anemometer propellor blades turning in the field of view can be a problem. Precipitation also effects the readings.

5. SATURATION OF SCINTILLATION

We have examined the effects of saturation of scintillation upon optical wind measurement both experimentally and by the application of the saturation theory developed earlier (Clifford, et. al. 1974). An example of the observed effects of saturation upon the active, laser-beam system, compared with the theoretical prediction, is shown in figure 21.

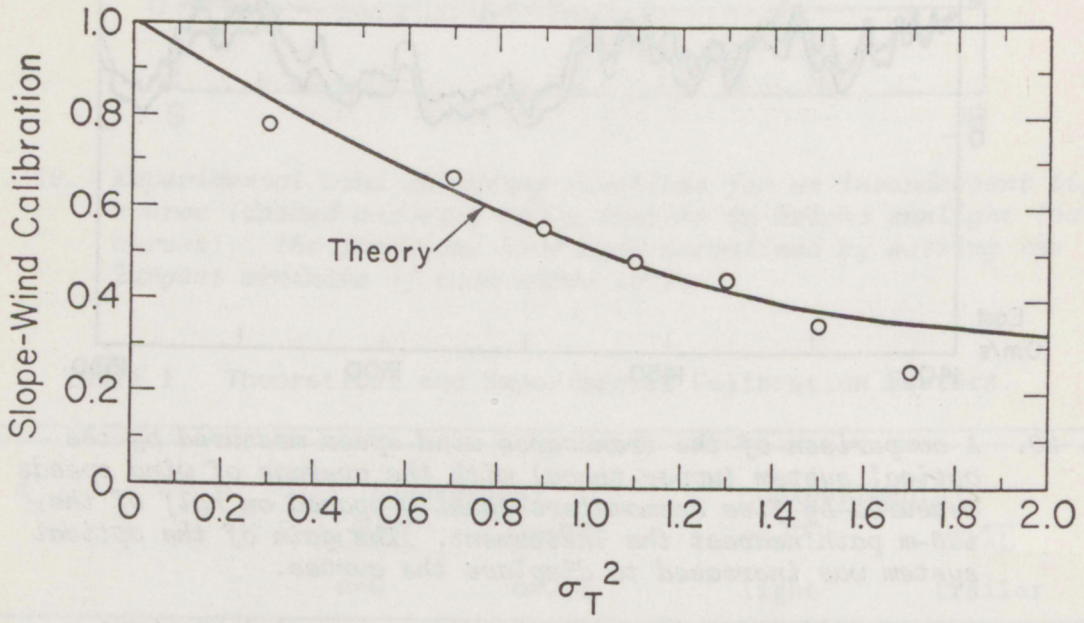

Fig. 21. Slope-wind calibration vs log-amplitude variance σ_t^2 predicted by the spherical wave propagation relationship. The solid lines are predicted from the saturation theory of Clifford et al. 1974. The experimental points have been obtained from measurements made in the σ_t^2 ranges indicated.

Though the effect upon the wind measurement is discouraging, the agreement with theory is gratifying. The new insight into the mechanism of saturation has allowed us to develop new techniques of optical wind measurement that largely overcome the saturation problem. The theory indicates that saturation will not have a major effect upon the passive wind system as long as the mode of operation is such that the principal turbulence sizes observed for the wind measurement are sufficiently large, compared to a Fresnel zone, at the path location in question. Since the

spectral content of a typical scene is similar to that of a large incoherent source, little saturation effect is anticipated.

6. DISCUSSION

An extensive experimental and theoretical exploration of different techniques for making an optical passive wind measurement has been made during the course of this project. A minor part of the project was then devoted to the design of a prototype instrument to demonstrate the feasibility of the most promising approach. Clearly, more effort devoted to the design of the instrument would better realize the potential of this technique. Specifically, the range of the instrument is limited by its aperture. The previously mentioned problems of obstruction of the secondary in a mirror system could be solved by proper geometrical arrangement, and larger apertures could be attained in mirror systems at relatively modest cost. More efficient use of the aperture could also be made, and smaller focal ratios with attendant advantages obtained. All of this would improve the S/N ratio and the range.

The scene spectral measurement is regarded more as an engineering problem than a fundamental limitation. With the solution of this measurement problem, the potential then exists for automatic control of the instrument. This would require extensive experience with a wide variety of naturally occurring scenes and a facility for synthesizing scenes with a known spectrum to provide an effective experimental check of the theory of operation. However, limitations will still exist with regard to scene movement and precipitation effects.

We conclude that the passive wind sensor has useful application but requires a more extensive demonstration of its ability to perform with a wider variety of scene spectra and under more diverse meteorological conditions before the technique becomes operational.

7. REFERENCES

Clifford, Steven F. (1971), Temporal frequency spectra for a spherical wave propagating through atmospheric turbulence, *J. Opt. Soc. Am. 61*: 1279-1284.

Clifford, S. F., G. R. Ochs, and R. S. Lawrence (1974), Saturation of optical scintillation by strong turbulence, *J. Opt. Soc. Am. 64*: 148-154.

Kolmogorov, A. N. (1941), The local structure of turbulence in incompressible viscous fluid for very large Reynolds' numbers, *Doklady Akad. Nauk SSSR 30:* 301. German translation in "Sammelband zur Statistichen Theorie der Turbulenz", *Akademie-Verlag*, Berlin (1958), p. 71.

Lawrence, R. S., G. R. Ochs, and S. F. Clifford (1972), The use of scintillations to measure average wind across a light beam, *Appl. Opt. 11*: 239-243.

Lee, R. W. and S. C. Harp (1969), Weak scattering in random media with application to remote sensing, *Proc. IEEE 57*: 375-406.

Ochs, G. R. and G. F. Miller (1972), Pattern velocity computer - two types developed for wind velocity measurement, *Rev. of Sci. Instr. 43*: 879-882.

Ochs, G. R., S. F. Clifford, and Ting-i Wang (1973), A feasibility study of an optical crosswind monitor, NOAA Tech. Memo ERL WPL-10.

Ochs, G. R.,G. F. Miller, and E. J. Goldenstein (1975), The NOAA passive optical crosswind monitor, NOAA Tech. Memo ERL WPL-11.

Tatarski, V. I. (1961), *Wave Propagation in a Turbulent Medium*, translated by R. S. Silverman, McGraw-Hill Book Co., Inc. New York, N. Y. 285 pp.

USCOMM - ERL

☆GPO 1974 — 677-238/1241 REGION NO. 8